Supplementary Information

Elucidating the mobility of H^+ and Li^+ ions in $(Li_{6.25-x}H_xAl_{0.25})La_3Zr_2O_{12}$ via correlating neutron and electron spectroscopy

Xiaoming Liu[#,1], Yan Chen[#,2], Zachary D. Hood[1,3], Cheng Ma[4], Seungho Yu[5], Asma Sharafi[5], Hui Wang[6], Ke An[2], Jeff Sakamoto[5], Donald J. Siegel,[5,7] Yongqiang Cheng*[,2], Niina H. Jalarvo*[,2], Miaofang Chi*[,1]

[1] Center for Nanophase Materials Sciences, Oak Ridge National Laboratory, Oak Ridge, TN 37831, USA

[2] Neutron Scattering Division, Oak Ridge National Laboratory, Oak Ridge, TN 37831, USA

[3] Department of Materials Science and Engineering, Massachusetts Institute of Technology, Cambridge, MA, USA

[4] School of Chemistry and Materials Science, University of Science and Technology of China (USTC), Hefei, Anhui 230026, China

[5] Mechanical Engineering, University of Michigan, Ann Arbor, MI 48109, USA

[6] Mechanical Engineering, Conn Center for Renewable Energy Research, University of Louisville, Louisville, KY, 40292, USA

[7]Department of Materials Science and Engineering,[8]Michigan Energy Institute, and [9]Applied Physics Program, University of Michigan, Ann Arbor, MI 48109, United States

[*] Corresponding authors: Miaofang Chi (chim@ornl.gov), Niina Jalarvo (jalarvonh@ornl.gov), and Yongqiang Cheng (chengy@ornl.gov)

Keywords: Aqueous lithium batteries, neutron scattering, proton exchange, proton mobility, solid electrolytes

Experimental Methods

Cubic-structured $(Li_{6.25}Al_{0.25})La_3Zr_2O_{12}$ powders were synthesized via solid-state reaction method following similar procedures as described elsewhere.[1] The synthesized powders (5.5 g) were submerged into 500 mL deionized water (pH = 5) and stirred to enable the Li^+/H^+ exchange reaction. The pH of the solution quickly increased to 13-14. In order to enhance the ion exchange extent, HNO_3 (0.01M) was slowly added to the solution until the pH was between 5 and 6, followed by stirring for 30 min. The powders were collected by vacuum filtration and were dried at room temperature on a high-vacuum Schlenk line for 12 hours. The pH was recorded by a pH meter (Denver Instruments Model 215).

(S)TEM and EELS investigations were carried out on an aberration-corrected FEI Titan S 80-300 TEM/STEM equipped with a Gatan Image Filter Quantum-865 operated at 300 kV. Electron energy-loss spectroscopy (EELS) was performed under STEM mode with a dispersion of 0.3 eV per channel and a 5mm aperture. The preparation of the LLZO TEM specimen is described elsewhere.[2] This entire process is water free in order to avoid surface reactions. The TEM specimens were maintained under vacuum for all sample preparation procedures. When the microscopy analysis of pristine LLZO was completed, (S)TEM and EELS examination was conducted on the HNO_3-treated H_x-LLZO with minimal exposure time to air.

Thermogravimetric analysis (TGA, TA Instruments Q500) of the HNO_3-treated LLZO powders was performed between 25-500 ^oC under a flow of N_2 (10 mL/ min) at a heating rate of 10 ^oC/min. the powders were baked at 80 ^oC for 24 hours to remove the moisture absorbed on LLZO surface before subsequent structural investigations. Such an annealing condition was chosen based on TGA analysis which shows that moisture can be nearly completely removed at such treatment, detailed information is shown in supplemental Fig. S2. Powder X-ray diffraction (XRD) patterns of pristine LLZO and protonated LLZO powders were collected using a PANalytical X'pert Pro diffractometer Fig. S3. Neutron powder diffraction of protonated LLZO was performed at the VULCAN instrument,[3,4] Spallation Neutron Source (SNS), Oak Ridge National Laboratory (ORNL). Rieveld refinement of the NPD was carried out using GSAS and EXPGUI.[5,6] Inelastic neutron spectroscopy measurements were performed at the VISION spectrometer, SNS, ORNL. Quasielastic neutron scattering measurements were carried out at the BASIS backscattering spectrometer, SNS, ORNL. Calculations were performed using density functional theory (DFT) with a plane wave basis set, as implemented in the Vienna *Ab initio* Simulation Package (VASP).[7]

Simulation Methods

Theoretical calculations were based on the cubic unit cell of LLZO (8 formula units, 192 atoms).[8] Li was randomly distributed on the partially-occupied 24d (tetrahedral Li(1)) and 96h (octahedral Li(2)) sites using a procedure which prohibited occupancy on electrostatically-unfavorable first nearest-neighbor sites. An earlier study[9] showed negligible energy differences (<1.5

meV/atom) among several LLZO structures generated in this manner. The LLZO structure having the lowest total energy was adopted for subsequent calculations. The partial occupancies of this structure were 0.542 and 0.448 (equivalent to 13 and 43 atoms in unit cell) for the 24d and 96h sites, respectively. These partial occupancies are similar to the experimental values of 0.564 and 0.442 for 24d and 96h sites, respectively.[8]

H-doped LLZO was prepared using seven different levels of proton concentration. Li atoms in the LLZO unit cell were substituted by H atoms, resulting in nominal compositions: $Li_{7-x}H_xLa_3Zr_2O_{12}$ with x= 0.625, 1.875, 3.125, 4.375, 5.625, 6.375, and 7. Site preference tests showed that substitution on 96h sites instead of 24d sites reduced the total energy about 5 and 20 meV/atom for $Li_{6.375}H_{0.625}La_3Zr_2O_{12}$ and $Li_{2.625}H_{4.375}La_3Zr_2O_{12}$, respectively. The structure with H substitution primarily on 96h sites was used for subsequent calculations. Lattice parameters for pure and H-doped LLZO were obtained by fitting total energy *vs.* volume data to the Murnaghan equation of state.[10]

All calculations were performed using density functional theory (DFT) with a plane wave basis set, as implemented in the Vienna *Ab initio* Simulation Package (VASP).[7] Core-valence electron interactions were treated using the projector augmented wave (PAW)[11,12] method, and the semi-local generalized gradient approximation (GGA) of Perdew, Burke, and Ernzerhof (PBE)[13] was used for the exchange-correlation energy. Ionic relaxations were conducted until the atomic forces were less than 0.03 eV/Å. The convergence criterion for the total energy in the electronic self-consistency loop was set to 10^{-5} eV. An energy cutoff of 600 eV was used for the plane wave basis, and the Brillouin zone was sampled using a Monkhorst-Pack[8] k-point grid with a 2 × 2 × 2 sampling density.

Figure S1 and Table S2 show the effect of protonation on the lattice constant of cubic LLZO as a function of proton exchange extent at 0 K. It demonstrates that the lattice constant for H_x-LLZO increases in an approximately linear fashion with increasing proton concentration. The calculated lattice constant for pure LLZO (13.03 Å) is in good agreement with the measured value (12.97 Å). Similarly, a good agreement is obtained at a proton concentration of approximately 70 % (as described above): 13.17 Å (calculated) vs. 13.07 Å (measured).

Figures

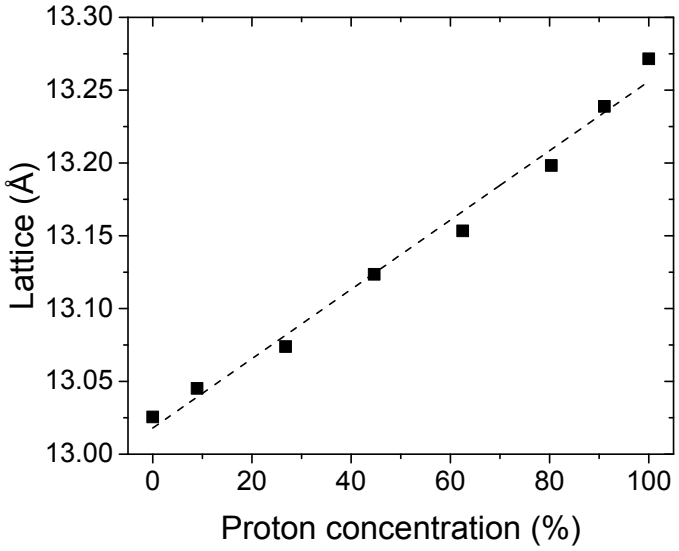

Figure S1. Lattice parameters for pure and H-doped LLZO as a function of proton concentration at zero Kelvin.

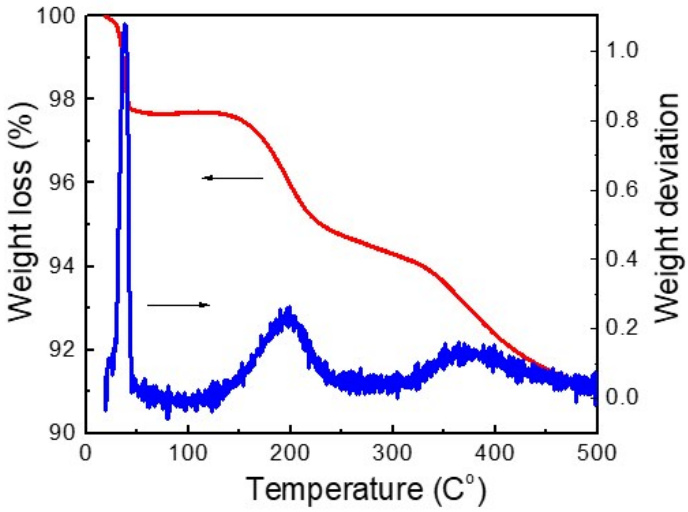

Figure S2. TGA analysis of H_x-LLZO in a temperature range between 25 °C and 500 °C.

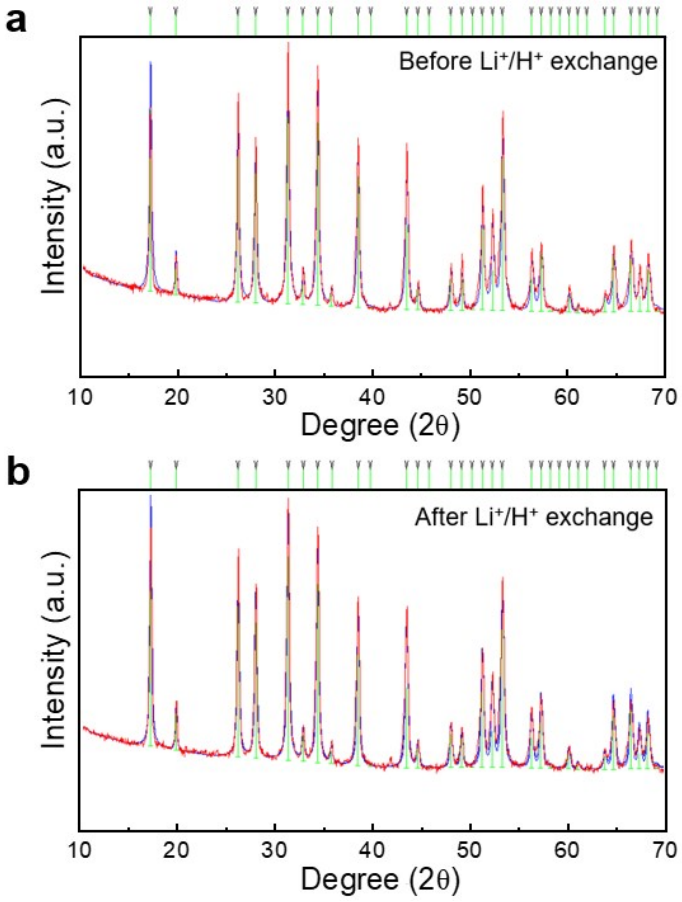

Figure S3 X-ray diffraction patterns of LLZO samples **a** before proton exchange and **b** after H exchange. The X-ray diffraction patterns are indexed to the cubic *Ia-3d* symmetry (space group: *m-3m*). The pristine LLZO has a lattice parameter of a = 12.9721(7) Å while the protonated LLZO has a lattice parameter of a = 12.9806(8) Å.

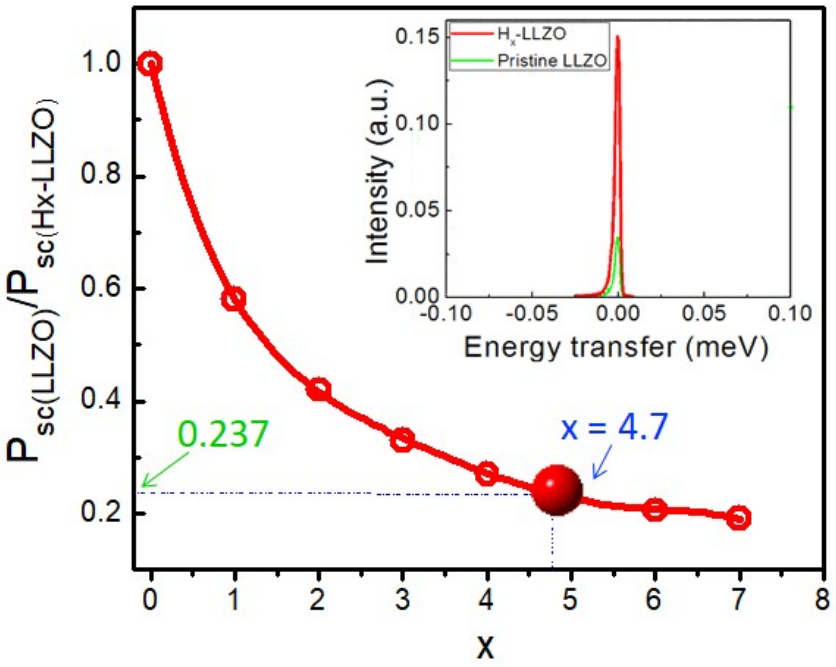

Figure S4. The calculated ratio of the scattering probability between LLZO and H_x-LLZO ($0 \leq x \leq 7$). Inset is the BASIS spectra over Q = 0.2 to 1 $Å^{-1}$free of Bragg peaks for both of the two studied samples. The spectra were integrated over the energy range ±100 meV, and then the ratio of the integrated scattering intensities (I_{sc}) was calculated to be 0.237, which is proportional to the ratio of scattering probability. The blue dashed line is interpolation to the experimentally observed value of 0.237, giving a H concentration of $x \approx 4.7$.

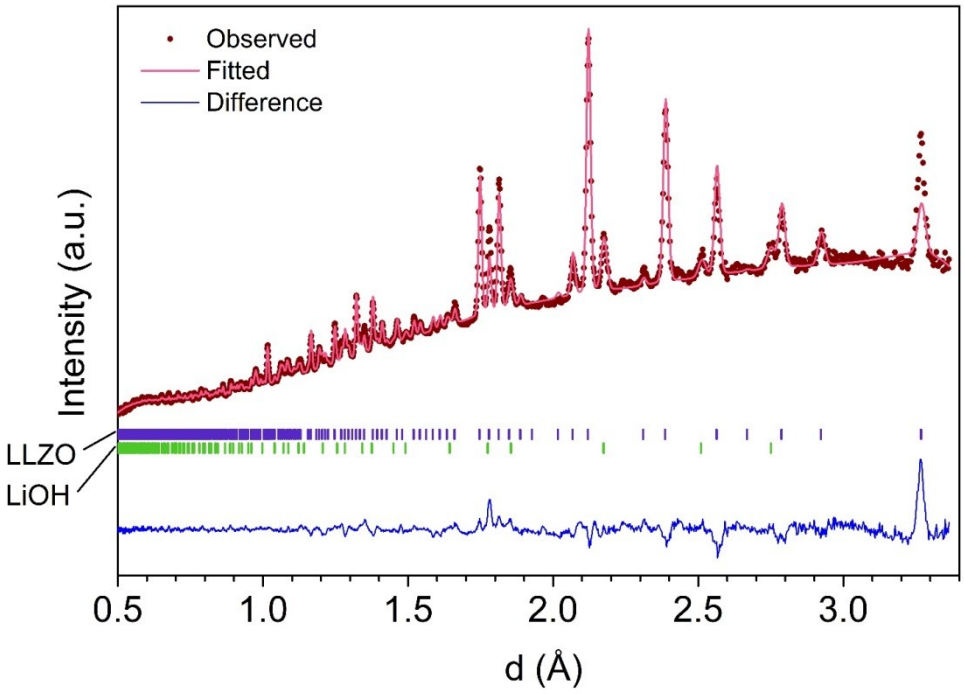

Figure S5. A trial of using *Ia-3d* structure model to fit the neutron diffraction pattern of protonated LLZO (χ^2 = 3.253, wRp = 0.0209, Rp = 0.0167), showing a worse fitting compared to Figure 2a using *I-43d* model.

Table S1. Refined structural parameters for protonated LLZO powders neutron diffraction data for the *I-43d* space group with a lattice parameter a = 13.0704(2). (χ^2 = 0.7522, wRp = 0.01, Rp = 0.0078)

Atom	Sites	X	Y	Z	Occupancy	U_{iso} (x100)
La	24d	0.1306(3)	0	0.25	1	1.10(5)
Zr	16c	0.0100(1)	0.0100(1)	0.0100(1)	1	1.50(8)
Li (1)	12a	0.25	0.375	0	0.34(6)	1.06(45)
Li (2)	12b	0.75	0.625	0	0.63(7)	1.06(45)
Al (1)	12a	0.25	0.375	0	0.0833	1.06(45)
Al (2)	12b	0.75	0.625	0	0.0833	1.06(45)
O (1)	48e	0.2858(3)	0.1071(2)	0.1956(3)	1	1.66(8)
O (2)	48e	0.7264(2)	0.9027(2)	0.8096(3)	1	1.08(7)
H	48e	0.3425(7)	0.3952(8)	0.0675(7)	0.78(3)	5.16(28)

Table S2. Lattice parameters and volumes of pure and H-doped LLZO as a function of proton concentration at zero Kelvin, obtained from DFT calculations.

	Composition	H^+ ratio (%)	Lattice (Å)	Volume (Å^3 / atom)
Pure-LLZO	$Li_7La_3Zr_2O_{12}$	0	13.026	11.512
5H-LLZO	$Li_{6.375}H_{0.625}La_3Zr_2O_{12}$	8.9	13.045	11.562
15H-LLZO	$Li_{5.125}H_{1.875}La_3Zr_2O_{12}$	26.8	13.074	11.639
25H-LLZO	$Li_{3.875}H_{3.125}La_3Zr_2O_{12}$	44.6	13.124	11.772
35H-LLZO	$Li_{2.625}H_{4.375}La_3Zr_2O_{12}$	62.5	13.153	11.852
45H-LLZO	$Li_{1.375}H_{5.625}La_3Zr_2O_{12}$	80.4	13.198	11.974
51H-LLZO	$Li_{0.625}H_{6.375}La_3Zr_2O_{12}$	91.1	13.239	12.085
56H-LLZO	$H_7La_3Zr_2O_{12}$	100	13.272	12.175

References:

1. Wolfenstine, J., Sakamoto, J. & Allen, J. L. Electron microscopy characterization of hot-pressed Al substituted Li7La3Zr2O12. *J. Mater. Sci.* **47,** 4428–4431 (2012).
2. Ma, C., Rangasamy, E., Liang, C., Sakamoto, J., More, K. L. & Chi, M. Excellent Stability of a Lithium-Ion-Conducting Solid Electrolyte upon Reversible Li^+/H^+ Exchange in Aqueous Solutions. *Angew. Chem.* **127,** 131–135 (2015).
3. An, K., Skorpenske, H. D., Stoica, A. D., Ma, D., Wang, X.-L. & Cakmak, E. First In Situ Lattice Strains Measurements Under Load at VULCAN. *Metall. Mater. Trans. A* **42,** 95–99 (2011).
4. Chen, Y., Rangasamy, E., dela Cruz, C. R., Liang, C. & An, K. A study of suppressed formation of low-conductivity phases in doped $Li_7La_3Zr_2O_{12}$ garnets by in situ neutron diffraction. *J Mater Chem A* **3,** 22868–22876 (2015).
5. Larson, A. C. & Von Dreele, R. B. General structure analysis system (GSAS). *Los Alamos Natl. Lab. Rep. LAUR* **55,** 86–748 (2004).
6. Toby, B. H. EXPGUI, a graphical user interface for GSAS. *J. Appl. Crystallogr.* **34,** 210–213 (2001).
7. Kresse, G. & Furthmüller, J. Efficient iterative schemes for *ab initio* total-energy calculations using a plane-wave basis set. *Phys. Rev. B* **54,** 11169–11186 (1996).
8. Xie, H., Alonso, J. A., Li, Y., Fernández-Díaz, M. T. & Goodenough, J. B. Lithium Distribution in Aluminum-Free Cubic Li7La3Zr2O12. *Chem. Mater.* **23,** 3587–3589 (2011).
9. Yu, S., Schmidt, R. D., Garcia-Mendez, R., Herbert, E., Dudney, N. J., Wolfenstine, J. B., Sakamoto, J. & Siegel, D. J. Elastic Properties of the Solid Electrolyte $Li_7La_3Zr_2O_{12}$ (LLZO). *Chem. Mater.* **28,** 197–206 (2016).
10. Murnaghan, F. D. The Compressibility of Media under Extreme Pressures. *Proc. Natl. Acad. Sci.* **30,** 244–247 (1944).
11. Blöchl, P. E. Projector augmented-wave method. *Phys. Rev. B* **50,** 17953–17979 (1994).
12. Kresse, G. & Joubert, D. From ultrasoft pseudopotentials to the projector augmented-wave method. *Phys. Rev. B* **59,** 1758–1775 (1999).
13. Perdew, J. P., Burke, K. & Ernzerhof, M. Generalized Gradient Approximation Made Simple. *Phys. Rev. Lett.* **77,** 3865–3868 (1996).